Moment-rotation behavior of welded tubular high strength steel T joint

Jarmo Havula[1], Marsel Garifullin[2], Markku Heinisuo[2], Kristo Mela[2], Sami Pajunen[2]

[1] *HAMK University of Applied Sciences, Hämeenlinna, Finland*

[2] *Tampere University of Technology, Tampere, Finland*

Abstract

Based on recent studies, high strength steels (HSS) can be efficiently used in civil engineering, reducing the consumption of material and CO_2 emissions. The present Eurocode contains the reduction coefficients (0.8 and 0.9 depending on the steel grade) for high strength steel joints. These reduction factors lead to the excessive consumption of material, making the usage of HSS for construction not as economically viable as they might be. In addition, the present Eurocode contains no method to determine the stiffness of hollow section joints. The scope of this paper is to present experimental results dealing with the welded in-plane moment-loaded HSS joints. Twenty tests on square hollow-section T joints were performed to observe their moment-rotation relationship, studying the following parameters: 1) bending resistance, 2) rotational stiffness, 3) ductility. The results show that the reduction factors are needed only for butt-welded joints, as well as for joints with small fillet welds and made of steel grades higher than S500. The required ductility was achieved by all the samples, even when using welds smaller than full-strength fillet welds. In addition, it was shown experimentally that fillet welds considerably increase the resistance and stiffness of joints.

Keywords

High strength steel, welded tubular T joint, in-plane moment-load, moment resistance, rotational stiffness, ductility, reduction coefficient.

Introduction

The application field for high strength steel (HSS) joints covers a wide range of structures, including bridges, lattice masts, and buildings. Hollow section joints subject to bending moment are found in beam-to-column connections or as a simple joint configuration in Vierendeel girders. The beam-to-column T joint is comprised of a brace member connected at an angle of 90° to a chord member.

The developments in manufacturing processes and material technologies increased the strength of available steels worldwide [1]. Generally, the steel grade $f_y \leq 355$ MPa is considered as regular steel, although basic Eurocodes EN 1993-1-1 to EN 1993-1-11 consider steel grades up to $f_y \leq 460$ MPa, where f_y is the yield strength. Following EN 1993-1-12:2007 [2], high strength steel (HSS) is defined as 460 MPa $< f_y \leq 700$ MPa. To make the usage of HSS in construction as viable as possible, more precise and accurate calculation methods should be developed for HSS structures. Attention should be paid particularly to the resistance and rotational stiffness of joints. The increase of joint resistance clearly reduces material consumption, while the increase of stiffness affects the load distribution in the structure and reduces the buckling length of members, contributing to the reduction of costs.

Currently, EN 1993-1-8:2005 [3] and EN 1993-1-12:2007 [2] contain additional rules for HSS joints. Following these rules, clause 7.1.1(4) of EN 1993-1-8:2005 requires using the factor 0.9 for the static design resistances of end-products with a nominal yield strength higher than 355 N/mm^2. This rule must be fulfilled for the design equations in Section 7; however, it does not concern the design of welds. In addition, clause 2.8 of EN 1993-1-12:2007 contains the reduction factor 0.8 for steel grades greater than S460 up to S700. The identical requirements can be found in the latest CIDECT Design Guide No.3 [4].

In the design of HSS joints, these factors considerably reduce the design resistance of joints, making their design very conservative.

Currently, there is no clear evidence regarding the origin of these reduction factors. It should be noted that the rules for HSS have been developed based on a very limited number of experiments for variable types of joints, especially when considering the full-scale HSS joints. The lack of experimental data could have led to the necessity to reduce the design resistance of HSS joints, leading to the introduction of these factors. According to [5] and the latest CIDECT Design Guide No.3 [4], the need for reduction factors can be explained by the relatively larger deformations that take place in joints with nominal yield strengths of approximately 450 to 460 MPa, when the plastification of the connecting RHS face occurs. A broad discussion on this issue can be found in [6]. Based on about 100 tests on HSS joints, it proposes no reduction for the steel grade S500, but implies the reduction factor 0.9 for the steel grade S700 when the connected brace is loaded with the axial load.

At the same time, the reduction can be also caused by the softening of the heat affected zone (HAZ) [7–9]. According to [8], the effect of weld-induced heat on the mechanical properties of steel tubes results in an overall reduction around of 8% in HSS. Dunđer et al. [10] present the $t_{8/5}$ cooling time–hardness relationship for TStE 420 steel HAZ softening, clearly indicating the importance of HAZ and weld-heat input when considering the resistance of HSS welded joints. However, both EN 1993-1-8:2005 and EN 1993-1-12:2007 require no reductions due to HAZ. Only the Finnish National Annex for EN 1993-1-12:2007 [11] contains a rule to reduce the yield strength, with the factors 1.0 for S500, 0.85 for S700 and linear interpolation in between. However, this reduction does not concern the design equations for hollow section joints in section 7 of EN 1993-1-8:2005. In any case, this issue remains open and requires more research for moment-loaded joints.

Another problem of HSS joints is the high price of welding when full-strength welds are used. According to [12], full-strength fillet welds result in extremely large throat thickness, namely $1.48t_1$ for S420, $1.61t_1$ for S500 and $1.65t_1$ mm for S700, where t_1 is the wall thickness of the connected tube. Such large welds increase the number of welding runs and thus, taking into account the high costs of welding, make the welding process extremely expensive for HSS. According to [6], the full-strength fillet-weld throat thicknesses can be reduced to $1.0t_1$ for S500, $1.2t_1$ for S700 and $1.4t_1$ for S960, provided that they can resist the loads.

Subsequent to the above discussion, the scope of this paper is to present the experimental results of welded moment-loaded HSS joints. Twenty tests on square hollow section T joints were performed to:

- observe the moment-rotation relationship in the whole range of loading: initial stiffness, hardening stiffness, plastic and ultimate moment resistances and ductility;
- determine the need for reduction coefficients and propose smaller ones, if possible;
- evaluate the effect of weld size on the moment resistance, initial rotational stiffness, and ductility of joints, and justify the use of welds that are smaller than full-strength ones.

The paper considers only joints with brace-to-chord width ratio $\beta = b_1/b_0 \leq 0.85$, i.e., when chord face bending governs the deformation of the specimen. Joints with fillet and butt welds are considered. Fig. 1 presents the typical moment-rotation relationship for a hollow section joint with $\beta \leq 0.85$. In the figure, $M_{pl,exp}$ and $M_{u,exp}$ denote plastic and ultimate moment resistances, respectively; $S_{j,ini}$ and $S_{j,h}$ denote initial and hardening rotational stiffness, respectively; φ_u denotes rotation corresponding to ultimate resistance. According to [13], for this type of joints plastic moment resistance $M_{pl,exp}$ is determined as the intersection of the two tangent lines corresponding to initial and hardening stiffness.

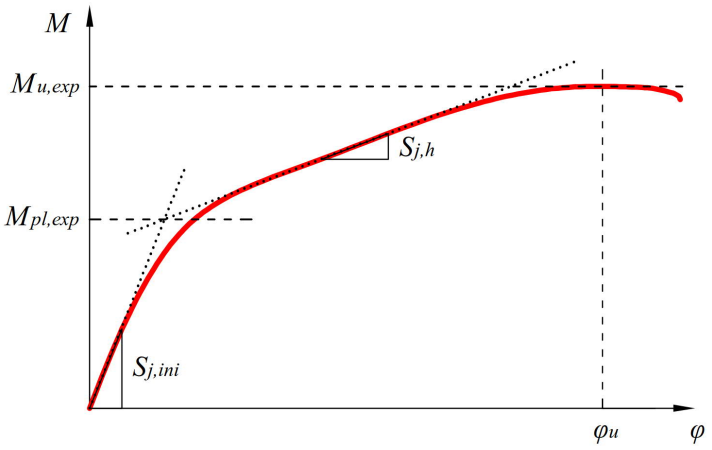

Fig. 1. Typical M-φ relationship for hollow section T joint with $\beta \leq 0.85$.

2. Literature review

2.1. Moment resistance

The first equations for strength of moment-loaded hollow section joints can be found in [14–17]. A comprehensive research on tubular joints was conducted by Wardenier [18], who first proposed the design formulae based on the classical yield line theory. Currently, these rules are used by many design standards, such as EN 1993-1-8:2005 [3], ISO 14346:2013 [19], and CIDECT Design Guide No.3 [4]. Some newer experimental tests are presented in [20, 21]. Tabuchi et al. [22] presented experimental results for in-plane moment loaded rectangular hollow section (RHS) T joints and examined their local failures. Szlendak [23] and Packer [24] developed design procedures for RHS connections under the moment loading. Intensive research for uniplanar and multiplanar RHS joints was conducted by Yu [25]. The deformation limit of RHS joints was investigated by Lu [26] and Zhao [27]. The comparison of conventional and bird-beak RHS joints under in-plane bending moment has been conducted in [28]. Cyclic tests on welded RHS connections were performed in [29]. Fatigue tests on hollow section joints made of HSS can be found in [30]. However, most of the presented tests have been conducted for regular steels; no experiments can be found for HSS tubular joints under static moment loading.

2.2. Rotational stiffness

In addition to moment resistance, rotational stiffness is an important quantity in the design of joints, needed particularly in a global analysis model based on beam elements. In addition, initial rotational stiffness has a great effect when cost optimal solutions are sought, both in sway frames [31–35] and non-sway frames [36]. Moreover, rotational stiffness was shown to have an influence on the buckling lengths of truss members [37–39]. Grotmann & Sedlacek [13] employed the component method to propose theoretical equations for the design of initial rotational stiffness of RHS T joints. Later, these equations were validated against experimental results in [40].

2.3. Ductility

The ductility requirements are not as straightforward as those for the moment resistance and initial stiffness, being dependent on the case. EN 1993-1-8:2005 and EN 1993-1-12:2007 provide the requirements for the basic steel material using the ultimate strain ε_u. Annex C of EN 1993-1-5:2006 [41] recommends a value of 5% for the principal strain at the ultimate limit state. To evaluate the ductility of members, the factor R, the ratio of plastic and elastic rotation, is used, being dependent on the layout of the frame and the loading conditions [42, 43]. A continuous beam with R = 3, the most unfavorable

system, is accepted in EN 1993-1-1:2005 as the minimum requirement for the members belonging to the cross-section class 1, allowing the global plastic design of the frame.

Rotation capacity has been studied by Beg et al. [45], who limited the rotation capacity of the entire joint by limiting the relevant principal strains of distinct components to 10-20%. EN 1998-1:2004 [46] proposes a general limit of 0.035 rad for joint rotation to fulfil the requirements for seismic design. This rule is aimed to allow joints form a sufficient plastic hinge to carry cyclic loads without brittle fracture in the connection [47].

For tubular joints, the ultimate deformation limit was proposed by Lu [26] to define the strength of joints that do not exhibit a pronounced peak load. Later it was discussed in [27] and [48]. Following this rule, the local displacement of the chord is limited to 3% of the width of the chord b_0. Applying this rule to moment-loaded joints, the rotation of the joint φ is limited to $\varphi_{lim,3\%} = 0.03b_0/(h_1/2)$, where h_1 is the height of the brace. This limit is based on the observation that hollow section joints that did exhibit a peak load had a corresponding local deformation of the chord face between 2.5-4% of b_0 [48]. Currently it is adopted by the International Institute of Welding (IIW) as the ultimate deformation limit to define and compare the strength of welded hollow section connections.

3. Experimental study

A total of twenty experiments with tubular T joints were performed at the Sheet Metal Centre at Häme University of Applied Sciences (HAMK), Finland. The specimens differed in steel grade, the size of welds and the type of welding. The brace of the specimen was welded at the midpoint of the chord at an angle of 90°, as shown in Fig. 2a. The brace-to-chord width ratio β varied from 0.67 to 0.80. Both the chord and the brace had a length of 700 mm. The 170x170x10 mm plates were welded at the ends of the chord, and 120x120x10 mm plates (140x140x10 for 120 mm brace) were welded at the ends of the brace, all made of S355 steel. The measured cross-section dimensions of the tubes are presented in Table 1, where the naming of the test specimens is presented in the format [chord material]_[brace material]_[weld type] and the measured dimensions follow the notations of Fig. 2b. The thicknesses (t_{m1}, t_{m2}, t_{m3}, t_{m4}) of the tubes were measured on the four sides of each tube. Radius r_m is an average value of the measured values. Three steel grades and their combinations were considered: S420, S500 and S700. Fig. 2 presents the details of steels and their properties obtained from tensile coupon tests.

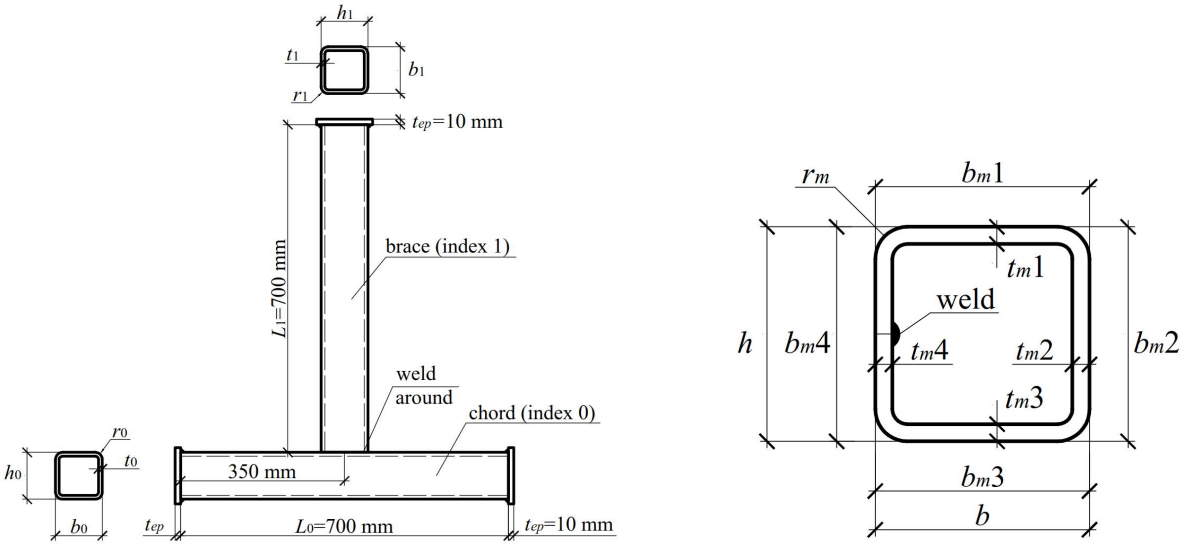

a) b)

Fig. 2. Test specimen: a) overall view, b) measured dimensions of tube. Plate 1 corresponds to compressed flange of brace.

Table 1. Measured section dimensions [mm].

Specimen	β	Member	Section	t_{m1}	t_{m2}	t_{m3}	t_{m4}	r_m	b_{m1}	b_{m3}	b_{m4}	b_{m2}
S420_S420_a6	0.67	Chord	150x150x8	7.88	8.00	7.95	8.07	21.00	151.70	151.70	151.30	151.30
		Brace	100x100x8	7.92	7.99	7.88	7.96	20.30	100.30	100.30	100.70	100.70
S500_S420_a6	0.67	Chord	150x150x8	7.89	8.05	7.90	8.03	19.50	149.60	149.60	150.00	150.00
		Brace	100x100x8	7.92	7.99	7.88	7.96	21.50	100.20	100.20	100.70	100.70
S500_S500_a6	0.67	Chord	150x150x8	7.89	8.05	7.90	8.03	20.50	149.90	149.90	151.50	151.50
		Brace	100x100x8	7.90	8.02	8.04	8.01	21.00	100.66	100.66	100.50	100.50
S700_S420_a6	0.67	Chord	150x150x8	7.84	7.95	7.89	7.97	19.50	150.70	150.70	151.60	151.60
		Brace	100x100x8	7.92	7.99	7.88	7.96	20.35	101.00	101.00	100.20	100.20
S700_S500_a6	0.67	Chord	150x150x8	7.84	7.95	7.89	7.97	19.50	150.60	150.60	150.90	150.90
		Brace	100x100x8	7.90	8.02	8.04	8.01	19.50	100.50	100.50	100.40	100.40
S700_S500_a6_WiPF	0.67	Chord	150x150x8	7.84	7.95	7.89	7.97	19.50	150.80	150.80	151.10	151.10
		Brace	100x100x8	7.90	8.02	8.04	8.01	19.50	100.60	100.60	100.55	100.55
S700_S700_a6	0.80	Chord	150x150x8	7.84	7.95	7.89	7.97	21.00	150.80	150.80	150.60	150.60
		Brace	120x120x8	7.96	7.96	8.01	7.96	20.50	120.60	120.60	120.40	120.40
S420_S420_a10	0.67	Chord	150x150x8	7.88	8.00	7.95	8.07	20.50	151.40	151.40	150.80	150.80
		Brace	100x100x8	7.92	7.99	7.88	7.96	20.00	100.94	100.94	100.33	100.33
S500_S420_a10	0.67	Chord	150x150x8	7.89	8.05	7.90	8.03	19.50	149.70	149.70	151.00	151.00
		Brace	100x100x8	7.92	7.99	7.88	7.96	20.50	100.80	100.80	100.30	100.30
S500_S500_a10	0.67	Chord	150x150x8	7.89	8.05	7.90	8.03	20.00	149.50	149.50	150.70	150.70
		Brace	100x100x8	7.90	8.02	8.04	8.01	19.50	100.50	100.50	100.40	100.40
S700_S420_a10	0.67	Chord	150x150x8	7.84	7.95	7.89	7.97	19.50	151.20	151.20	151.50	151.50
		Brace	100x100x8	7.92	7.99	7.88	7.96	22.00	100.80	100.80	100.15	100.15
S700_S500_a10	0.67	Chord	150x150x8	7.84	7.95	7.89	7.97	20.00	150.90	150.90	151.80	151.80
		Brace	100x100x8	7.90	8.02	8.04	8.01	20.00	100.60	100.60	100.50	100.50
S700_S500_a10_WiPF	0.67	Chord	150x150x8	7.84	7.95	7.89	7.97	20.50	151.20	151.20	151.90	151.90
		Brace	100x100x8	7.90	8.02	8.04	8.01	21.50	100.58	100.58	100.64	100.64
S700_S700_a10	0.80	Chord	150x150x8	7.84	7.95	7.89	7.97	20.50	150.50	150.50	151.30	151.30
		Brace	120x120x8	7.96	7.96	8.01	7.96	20.50	120.64	120.64	120.60	120.60
S420_S420_1/2v	0.67	Chord	150x150x8	7.88	8.00	7.95	8.07	20.50	150.60	150.60	151.60	151.60
		Brace	100x100x8	7.92	7.99	7.88	7.96	20.50	100.33	100.33	100.85	100.85
S500_S420_1/2v	0.67	Chord	150x150x8	7.89	8.05	7.90	8.03	19.50	149.70	149.70	150.30	150.30
		Brace	100x100x8	7.92	7.99	7.88	7.96	19.50	100.84	100.84	100.35	100.35
S500_S500_1/2v	0.67	Chord	150x150x8	7.89	8.05	7.90	8.03	20.50	149.60	149.60	151.40	151.40
		Brace	100x100x8	7.90	8.02	8.04	8.01	21.00	100.60	100.60	100.58	100.58
S700_S420_1/2v	0.67	Chord	150x150x8	7.84	7.95	7.89	7.97	20.00	150.70	150.70	151.70	151.70
		Brace	100x100x8	7.92	7.99	7.88	7.96	18.50	100.85	100.85	99.90	99.90
S700_S500_1/2v	0.67	Chord	150x150x8	7.84	7.95	7.89	7.97	20.50	150.50	150.50	151.70	151.70
		Brace	100x100x8	7.90	8.02	8.04	8.01	18.50	100.16	100.16	101.46	101.46
S700_S700_1/2v	0.80	Chord	150x150x8	7.84	7.95	7.89	7.97	19.50	150.10	150.10	150.90	150.90
		Brace	120x120x8	7.96	7.96	8.01	7.96	19.00	121.50	121.50	120.50	120.50

Three weld types, a6 and a10 fillet welds and 1/2v butt welds, were selected to determine the effect of the weld type and size on the resistance and stiffness of the joints (Table 3). The 1/2v butt welds were performed following EN ISO 9692-1:2013 [49], with no root support and with an 8 mm deep bevel all around the end of the brace (Fig. 3). The bevel shape complied with EN ISO 9692-1:2013, Table 1, Ref. No. 1.9.1, meaning a zero air gap (allowed max 2–4 mm) and a 45° angle (allowed 35–60°). However, the rules were violated in terms of the zero peak (straight part) at the bevel end (allowed 1-2 mm). The groove support was made by welding firstly a small weld at the groove tip, followed by the final load-bearing weld.

Table 2. Measured material properties.

Specimen	Chord	E_0 [GPa]	f_{y0} [MPa]	f_{u0} [MPa]	Brace	E_1 [GPa]	f_{y1} [MPa]	f_{u1} [MPa]
S420_S420_a6	S420	185	507	562	S420	181	502	557
S500_S420_a6	Optim 500 MH	196	602	662	S420	181	502	557
S500_S500_a6	Optim 500 MH	196	602	662	Optim 500 MH	185	563	627
S700_S420_a6	Optim 700 Plus MH	197	769	850	S420	181	502	557
S700_S500_a6	Optim 700 Plus MH	197	769	850	Optim 500 MH	185	563	627
S700_S500_a6_WiPF	Optim 700 Plus MH	197	769	850	Optim 500 MH	185	563	627
S700_S700_a6	Optim 700 Plus MH	197	769	850	Optim 700 Plus MH	199	734	854
S420_S420_a10	S420	185	507	562	S420	181	502	557
S500_S420_a10	Optim 500 MH	196	602	662	S420	181	502	557
S500_S500_a10	Optim 500 MH	196	602	662	Optim 500 MH	185	563	627
S700_S420_a10	Optim 700 Plus MH	197	769	850	S420	181	502	557
S700_S500_a10	Optim 700 Plus MH	197	769	850	Optim 500 MH	185	563	627
S700_S500_a10_WiPF	Optim 700 Plus MH	197	769	850	Optim 500 MH	185	563	627
S700_S700_a10	Optim 700 Plus MH	197	769	850	Optim 700 Plus MH	199	734	854
S420_S420_1/2v	S420	185	507	562	S420	181	502	557
S500_S420_1/2v	Optim 500 MH	196	602	662	S420	181	502	557
S500_S500_1/2v	Optim 500 MH	196	602	662	Optim 500 MH	185	563	627
S700_S420_1/2v	Optim 700 Plus MH	197	769	850	S420	181	502	557
S700_S500_1/2v	Optim 700 Plus MH	197	769	850	Optim 500 MH	185	563	627
S700_S700_1/2v	Optim 700 Plus MH	197	769	850	Optim 700 Plus MH	185	734	854

1) E_0 is the Young's modulus of the chord.
2) f_{y0} is the yield strength of the chord.
3) f_{u0} is the ultimate strength of the chord.
4) E_1 is the Young's modulus of the brace.
5) f_{y1} is the yield strength of the brace.
6) f_{u1} is the ultimate strength of the brace.

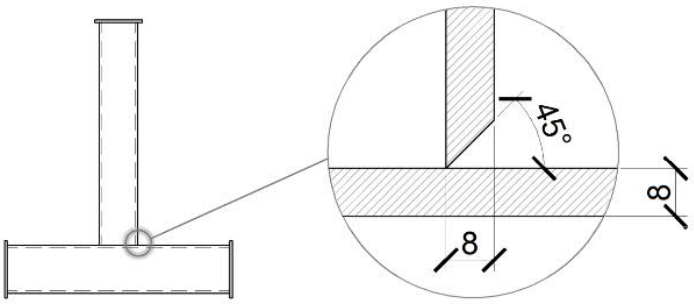

Fig. 3. 1/2v bevel welds.

The fillet weld sizes a_w were chosen to be less than the required full-strength weld sizes $a_{w,fs}$. This can be justified by clause 7.3.1 (6) of EN 1993-1-8:2005, which states: "The criterion given in 7.3.1(4) may be waived where a smaller weld size can be justified both with regard to resistance and with regard to deformation capacity and rotation capacity." The throat thicknesses were selected so that for some joints (a6 joints) the design resistance of welds was knowingly lower than the moment resistance based on the chord face failure, while for others (a10 joints) it was higher. The throat thicknesses of the full-strength fillet welds were determined according to [12]: $a_{w,fs} = 1.48t_1$ for S420, $a_{w,fs} = 1.61t_1$ for S500 and $a_{w,fs} = 1.65t_1$ for S700; where $t_1 = 8$ mm is the thickness of the brace. The ratio $a_w / a_{w,fs}$ is provided in Table 3.

Table 3. Weld properties.

Specimen	Welding process and position	Weld	a_w [mm]	$a_{w,fs}$ [mm]	a_w / $a_{w,fs}$
S420_S420_a6	MAG & PB	a6	6	11.9	0.51
S500_S420_a6	MAG & PB	a6	6	11.9	0.51
S500_S500_a6	MAG & PB	a6	6	12.9	0.47
S700_S420_a6	MAG & PB	a6	6	11.9	0.51
S700_S500_a6	MAG & PB	a6	6	12.9	0.47
S700_S500_a6_WiPF	MAG Wise & PB+PF	a6	6	12.9	0.47
S700_S700_a6	MAG & PB	a6	6	13.2	0.45
S420_S420_a10	MAG & PB	a10	10	11.9	0.84
S500_S420_a10	MAG & PB	a10	10	11.9	0.84
S500_S500_a10	MAG & PB	a10	10	12.9	0.78
S700_S420_a10	MAG & PB	a10	10	11.9	0.84
S700_S500_a10	MAG & PB	a10	10	12.9	0.78
S700_S500_a10_WiPF	MAG Wise & PB+PF	a10	10	12.9	0.78
S700_S700_a10	MAG & PB	a10	10	13.2	0.76
S420_S420_1/2v	MAG & PB	1/2v	-	-	-
S500_S420_1/2v	MAG & PB	1/2v	-	-	-
S500_S500_1/2v	MAG & PB	1/2v	-	-	-
S700_S420_1/2v	MAG & PB	1/2v	-	-	-
S700_S500_1/2v	MAG & PB	1/2v	-	-	-
S700_S700_1/2v	MAG & PB	1/2v	-	-	-

Two welding processes were used: MAG (manual welding) and MAG Wise (manual welding with Wise features), developed by Kemppi Oy (Lahti, Finland) and used for robot welding. The welding positions PB and PF were determined following DIN EN ISO 6947. The specimens were welded by a certified welder, following the instructions of the steel manufacturer in terms of heat input, weld speed, and cooling time $t_{8/5}$ to obtain the required strength of the weld. All filler materials were over-matching, meaning that the yield strength of the filler materials was larger than the base material in all the tests. The actual weld sizes were not measured and all the calculations were performed using the nominal values.

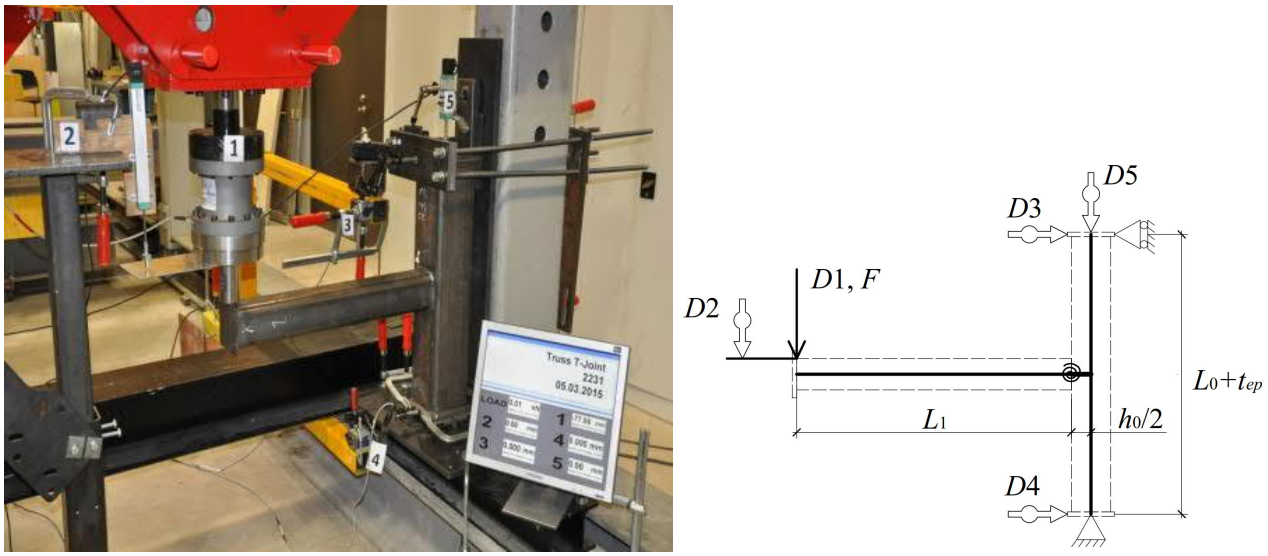

a) b)

Fig. 4. Test setup: a) test arrangement overview, b) static model of test specimen.

Fig. 4 shows the test setup and the static model of the test specimen with the locations of the displacement transducers and the load cell. The corresponding measured displacements are denoted as v_{D1}, v_{D2}, v_{D3}, v_{D4} and v_{D5}. Transducers *D*1 and *D*2 measured the same displacement. Transducer *D*1 was located inside the hydraulic cylinder. Transducer *D2* was supported from the floor and was used to validate transducer *D*1, since the hydraulic cylinder could move up under high loads, increasing the values of transducer *D*1. The force *F* was measured by the load cell installed at the head of the hydraulic cylinder (max load 250 kN). All the tests were displacement-controlled, with the 20 mm/min loading speed.

The vertical displacement at the end of the brace δ_b was calculated according to Eq. (1), subtracting the following from displacement v_{D1}:

1) the axial displacement v_{D5}, corresponding to the vertical displacement of the upper end of the specimen in relation to the floor, as shown in Fig. 5a.
2) the rigid body motion of the test specimens δ_{rb} due to the displacements at the supports v_{D3} and v_{D4}, as shown in Fig. 5b.

$$\delta_b = v_{D1} - v_{D5} - \delta_{rb} = v_{D1} - v_{D5} - \frac{L_1 + h_0/2}{L_0 + t_{ep}} \cdot \left(v_{D4} - v_{D3}\right) \tag{1}$$

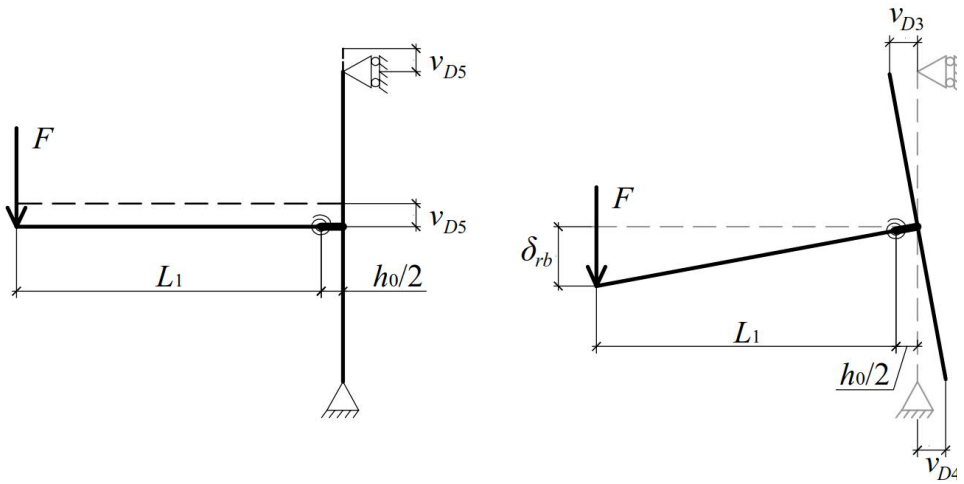

a) b)

Fig. 5. Corrections to calculate the displacement at the end of the brace: a) axial deformation of the chord, b) motion of the supports.

The local rotation of the joint φ was defined at the point where the brace was connected to the face of the chord. Generally, displacement δ_b corresponds to the global behavior of the specimen, which incorporates three simultaneous processes: the elastic bending of the brace (Fig. 6a), the elastic bending of the chord (Fig. 6b) and the local deformation of the joint (Fig. 6c). The latter is used to evaluate the moment-rotation behavior of the joint. Therefore, to obtain the local rotation of the joint φ, the displacement δ_b was reduced by the displacement due to elastic bending of the brace δ_{db} and the displacement due to elastic bending of the chord δ_{dc}:

$$\varphi = \frac{\delta_b - \delta_{db} - \delta_{dc}}{L_1} \tag{2}$$

Displacements of the brace and the chord were found according to the equations from strength of materials:

$$\delta_{db} = \frac{FL_1^3}{3EI_1} \tag{3}$$

$$\delta_{dc} = \frac{M}{3L_0^2 EI_0} \cdot \left[\left(\frac{L_0}{2} \right)^3 + \left(\frac{L_0}{2} \right)^3 \right] \cdot \left(L_1 + \frac{h_0}{2} \right) \tag{4}$$

where E is the Young's modulus of steel; I_1 and I_0 are correspondingly the second moments of inertia of the brace and the chord; $M = F \cdot (L_1 + h_0/2)$ is the bending moment defined at the line where the brace is connected to the center line of the chord. It should be noted that the paper does not consider the second order effects due to the deflection of the chord (e.g., the horizontal movement of the loading point), as well as the shear deflection of the connected members.

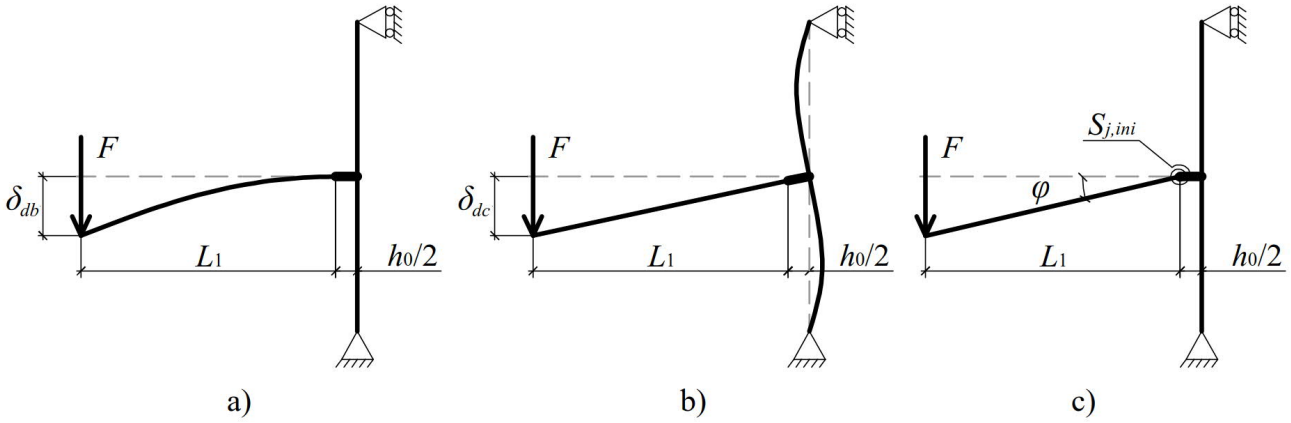

Fig. 6. Behavior of joint under loading: a) bending of brace; b) bending of chord; c) local deformation of joint.

4. Theoretical calculations

4.1. Design moment resistance

Generally, the structural behavior of tubular joints is complicated by non-uniform stress distribution over the surface of the chord. As it is shown in [18], elastic stress distribution becomes particularly non-uniform for joints with small β, sharply increasing in the corners of the brace. For this reason, an analytical solution for joint resistance is very complicated and is generally replaced by a semi-analytical approach, which assumes uniform distribution [18]. Moreover, as the stress level reaches plastic limit and initiate plastic deformations, the stress distribution becomes more uniform, justifying the adopted assumption.

According to EN 1993-1-8:2005, the deformation of RHS T joints with $\beta < 0.85$ is governed by chord face failure. Since the specimens had welds smaller than full-strength welds, the resistance of welds was also checked. In accordance with the foregoing, the moment joint resistance was found by

$$M_{j,Rd} = \min \left\{ M_{ip,1,Rd}, M_{w,Rd} \right\} \tag{5}$$

where $M_{ip,1,Rd}$ is the bending moment resistance based on chord face failure and $M_{w,Rd}$ is the bending moment resistance based on weld failure.

4.1.1 Moment resistance based on chord face failure

The moment resistance based on chord face failure $M_{ip,1,Rd}$ was calculated according to Table 7.14 of EN 1993-1-8:2005, with the measured yield strengths and the section dimensions and taking into account the reduction factor k_{HSS}:

$$M_{ip,1,Rd} = k_n f_{y0} k_{HSS} t_0^2 h_1 \left(\frac{1}{2\eta} + \frac{2}{\sqrt{1-\beta}} + \frac{\eta}{1-\beta} \right) / \gamma_{M5}, \tag{6}$$

where k_n is the chord stress function (not needed in this case), k_{HSS} is the reduction factor for HSS, $\beta = b_1/b_0$ is the brace-to-chord width ratio, $\eta = h_1/b_0$ is the brace height-to-chord width ratio. In keeping with the conditions for the reduction factors determined in the Introduction, they would take the following values (the given steel grades refer to the chord):

$$k_{HSS} = \begin{cases} 0.9, & \text{S420} \\ 0.8, & \text{S500, S700} \end{cases} \tag{7}$$

4.1.2 Moment resistance based on fillet-weld failure

In this paper, the design resistance of fillet welds is determined using the Directional method presented in EN 1993-1-8:2005. The welds related to b_1 are assumed to carry only the axial force P, while the welds related to h_1 are assumed to carry the shear load (Fig. 7a).

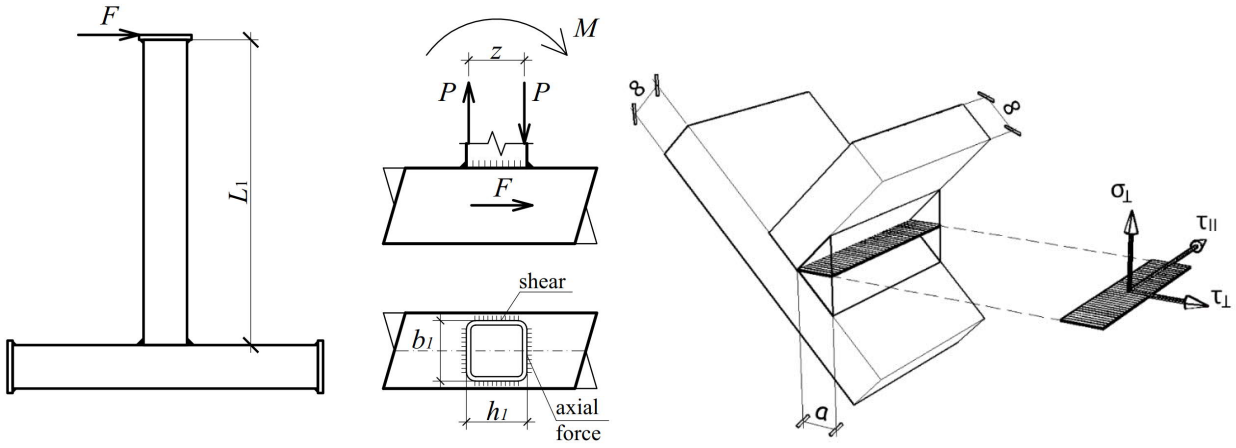

a) b)

Fig. 7. Design of welds: a) load components; b) stress components in weld.

The load P acting on the weld:

$$P = \frac{M}{z} = \frac{M}{h_1 - t_1}, \tag{8}$$

where the lever arm $z = h_1 - t_1$ is taken from EN 1993-1-8:2005, Figure 6.15.

The stress is calculated by dividing P by the throat area A_w (EN 1993-1-8:2005, 4.5.3.2(2)):

$$\sigma_w = \frac{P}{A_w} = \frac{P}{ab_1} = \frac{M}{ab_1(h_1 - t_1)} \tag{9}$$

Stresses acting on the weld (Fig. 7b):

$$\sigma_\perp = \tau_\perp = \frac{\sigma_w}{\sqrt{2}} \tag{10}$$

The design resistance of the fillet weld is sufficient if the following is satisfied (EN 1993-1-8:2005, 4.5.3.2(6)):

$$\sqrt{\sigma_\perp^2 + 3\left(\tau_\perp^2 + \tau_\parallel^2\right)} \le \frac{f_u}{\beta_w \gamma_{M2}}, \tag{11}$$

where β_w = 1 is the correlation factor for steel grades higher or equal to S420 and f_u is the minimum ultimate strength.

By putting (10) to (11):

$$\sigma_w = \frac{f_u}{\gamma_{M2}\sqrt{2}} \tag{12}$$

Equalizing (9) to (12):

$$\frac{M_{w,N,Rd}}{ab_1(h_1 - t_1)} = \frac{f_u}{\gamma_{M2}\sqrt{2}} \tag{13}$$

Thus, the moment resistance of the weld for normal stresses:

$$M_{w,N,Rd} = \frac{1}{\sqrt{2}} ab_1(h_1 - t_1)\frac{f_u}{\gamma_{M2}} \tag{14}$$

In the case of shear force, only the shear stress acts on the throat area:

$$\tau_{\parallel} = \frac{F}{A_w} = \frac{F}{2ah_1} \tag{15}$$

Eq. (11) takes the form:

$$\tau_{\parallel} = \frac{f_u}{\gamma_{M2}\sqrt{3}} \tag{16}$$

Equalizing (15) to (16):

$$F = \frac{2}{\gamma_{M2}\sqrt{3}} ah_1 f_u \tag{17}$$

The moment resistance of the weld for shear stresses:

$$M_{fw,S,Rd} = FL_1 = \frac{2}{\sqrt{3}} ah_1 \frac{f_u}{\gamma_{M2}} L_1 \tag{18}$$

The fillet weld final resistance is the minimum of the two:

$$M_{fw,Rd} = \min\left\{M_{fw,N,Rd}, M_{fw,S,Rd}\right\} \tag{19}$$

4.1.3 Moment resistance based on 1/2v butt weld failure

Similar to fillet welds, the design resistance of 1/2v butt welds is determined using the Directional method and the same assumptions. For the 1/2v butt weld, the stress components are found by

$$\sigma_{\perp} = \sigma_w; \quad \tau_{\perp} = \tau_{\parallel} = 0 \tag{20}$$

By putting (20) to (11):

$$\sigma_w = \frac{f_u}{\beta_w \gamma_{M2}}, \tag{21}$$

Equalizing (9) to (21):

$$\frac{M_{bw,Rd}}{ab_1(h_1 - t_1)} = \frac{f_u}{\gamma_{M2}} \tag{22}$$

Taking into account $a = t_1$, the bending resistance of the butt weld is found by

$$M_{bw,Rd} = \frac{f_u t_1 b_1 (h_1 - t_1)}{\gamma_{M2}} \tag{23}$$

4.2. Rotation capacity

As mentioned in the Introduction, the rotation limit for the joints is calculated according to the 3% deformation rule of Lu [26] leading to the following rotation limit:

$$\varphi_{\lim,3\%} = \frac{0.03 \cdot b_0}{h_1 / 2} = \frac{0.06}{\eta} \tag{24}$$

5. Results

All twenty tests were performed until the overall failure of the specimens. Since all the joints had the brace-to-chord width ratio in the range $\beta < 0.85$, their deformation was governed by chord face failure, as shown in Fig. 8a. In addition, chord side walls buckling was observed as the minor failure mode in all specimens (Fig. 8b). Strain hardening and the membrane effect allowed considerable post-yielding behavior. Finally, cracking in HAZ led the specimens to punching shear failure, as shown in Fig. 8c.

a) b) c)

Fig. 8. Observed failure modes: a) chord face failure; b) chord side walls failure; c) punching shear.

Graphically, the behavior of T joints can be presented by a corresponding moment-rotation (M-φ) curve. As an example, the M-φ response for case S700_S500_a6 is shown in Fig. 9; the remaining moment-rotation curves are provided in Appendix. The presented curves for all the joints are found to be similar to that shown in Fig. 1, with the following clearly observed phases:

- linear elastic phase, corresponding to elastic deformations with initial rotational stiffness $S_{j,ini}$;
- transitional phase, when the yielding of the joint starts and the slope starts to reduce;
- hardening phase, corresponding to hardening stiffness $S_{j,h}$;
- final failure, when the load starts to drop, corresponding to the failure in HAZ or weld.

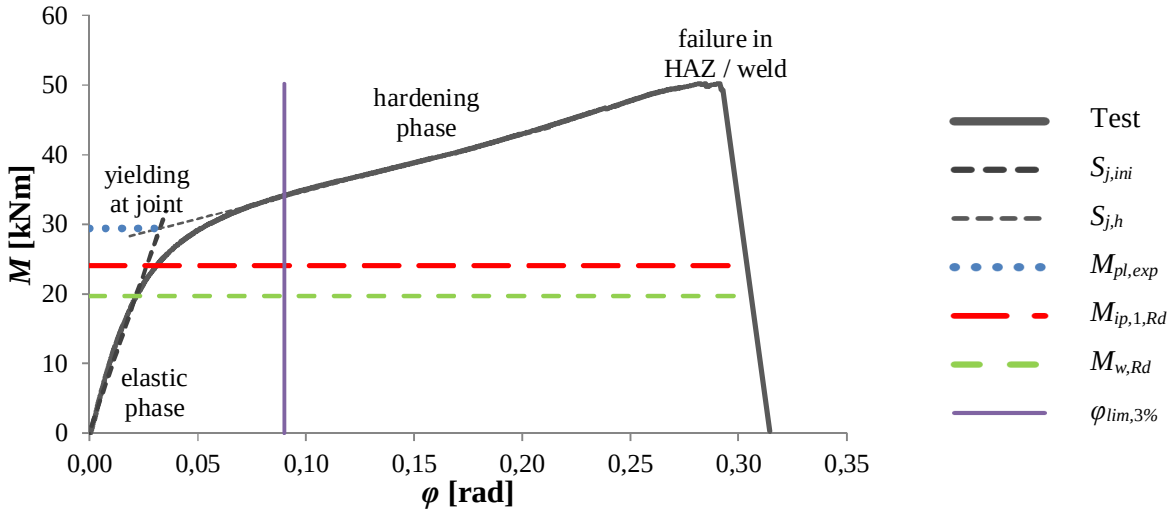

Fig. 9. Moment-rotational curve, specimen S700_S500_a6.

The following parameters were extracted from the test data and are summarized in Table 4:

- $S_{j,ini}$, initial joint stiffness (defined by the manual curve fitting);
- $S_{j,h}$, joint stiffness at the hardening phase (defined by the manual curve fitting);
- $M_{pl,exp}$, plastic moment resistance (determined according to Fig. 1);
- $M_{u,exp}$, ultimate moment resistance;
- φ_u, rotation corresponding the ultimate moment resistance.

Table 4. Experimental results.

Specimen	β	Weld	$M_{pl,exp}$ [kNm]	$M_{u,exp}$ [kNm]	φ_u [rad]	$S_{j,ini}$ [kNm/rad]	$S_{j,h}$ [kNm/rad]
S420_S420_a6	0.66	a6	21.2	34.6	0.270	866	56
S500_S420_a6	0.67		24.3	38.6	0.235	939	68
S500_S500_a6	0.67		25.0	39.3	0.227	861	69
S700_S420_a6	0.67		27.7	41.6	0.212	926	86
S700_S500_a6	0.67		29.4	50.2	0.283	900	80
S700_S500_a6_WiPF	0.67		31.2	39.5	0.147	888	79
S700_S700_a6	0.80		61.2	67.5	0.111	2052	82
S420_S420_a10	0.67	a10	31.6	48.7	0.263	1255	71
S500_S420_a10	0.67		35.1	57.3	0.302	1285	78
S500_S500_a10	0.67		37.2	48.1	0.201	1369	69
S700_S420_a10	0.67		38.5	53.4	0.201	1310	91
S700_S500_a10	0.67		45.5	58.0	0.175	1525	89
S700_S500_a10_WiPF	0.67		37.6	51.8	0.201	1295	84
S700_S700_a10	0.80		70.1	76.0	0.102	2551	96
S420_S420_1/2v	0.67	1/2v	18.5	27.4	0.218	750	54
S500_S420_1/2v	0.67		21.1	33.4	0.230	695	60
S500_S500_1/2v	0.67		21.0	28.0	0.177	845	60
S700_S420_1/2v	0.67		24.2	33.9	0.160	763	76
S700_S500_1/2v	0.67		26.4	39.8	0.211	816	72
S700_S700_1/2v	0.81		46.8	50.7	0.085	1694	70

The joints with β = 0.80 (cases S700_S700_a6, S700_S700_a10 and S700_S700_1/2) had a considerably smaller hardening phase than the joints with β = 0.67. This can be explained by the different influence of β on the resistance of joints: for higher β plastic resistance increases more radically than the resistance of welds. This leads to smaller post-yielding behavior of the joint. For this reason, the manual curve-fitting approach was not so straightforward for these cases and allowed several possible solutions to determine the corresponding hardening stiffness.

To investigate the dependence of plastic resistance on brace-to-chord width ratio β, it was normalized in respect to steel grade and geometry. Fig. 10a presents non-dimensional plastic moment resistance $M_{pl,exp}/(f_{y0}\cdot t_0^2\cdot h_1)$ in relation to β; for convenience, the points are grouped by weld size. The experimental results are compared to the theoretical equation, which is derived from Eq. (6) ($\eta = \beta$ in all cases):

$$f(\beta,\eta)=\frac{M_{ip,1,Rd}}{f_{y0}t_0^2h_1}=\frac{1}{2\eta}+\frac{2}{\sqrt{1-\beta}}+\frac{\eta}{1-\beta} \tag{25}$$

Fig. 10b presents the experimental plastic resistance normalized in relation to joint geometry $M_{pl,exp}/(t_0^2\cdot h_1\cdot f(\beta,\eta))$ and plotted against chord yield strength f_{y0}. The experimental results are compared to the theoretical equation, which in this case represents a linear regression:

$$f(f_{y0})=\frac{M_{ip,1,Rd}}{t_0^2h_1f(\beta,\eta)}=f_{y0} \tag{26}$$

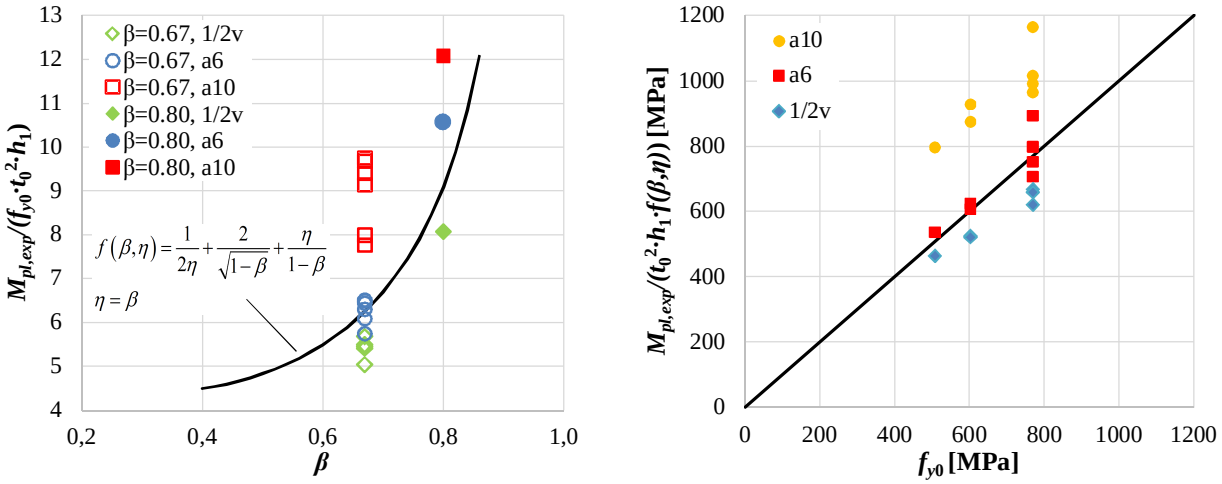

a) b)

Fig. 10. a) $M_{pl,exp}/(f_{y0}\cdot t_0^2\cdot h_1)$ in relation to β; b) $M_{pl,exp}/(t_0^2\cdot h_1\cdot f(\beta,\eta))$ in relation to f_{y0}.

As can be seen from Fig. 10, the experimental results confirm the general trend: brace-to-chord width ratio β significantly affects the resistance of joints representing the main factor in their structural behavior. Moreover, the results prove the linear dependence of plastic resistance on chord yield strength. In both cases, resistance is found dependent on welds: the joints with a10 fillet welds have significantly higher resistance than those with a6 mm; the latter have higher resistance than those with butt welds. This can be explained by the fact that fillet welds enlarge the cross-section of the brace at the connection area, increasing thus the total length of the yielding mechanism and leading to higher plastic resistance. No trend was observed in relation to the influence of brace material on the resistance of joints.

The theoretical moment resistances based on the chord face failure were calculated according to Section 3, with and without the reduction factor k_{HSS}. All the theoretical data are collected in Table 5 with the following notations:

- $M_{ip,1,Rd}$, the bending moment resistance based on the chord face failure (current Eurocode rules);
- $M^*_{ip,1,Rd}$, the bending moment resistance based on the chord face failure without k_{HSS};
- $M_{w,Rd}$, the bending moment resistance based on the weld failure ($M_{fw,Rd}$ or $M_{bw,Rd}$);
- $M_{j,Rd}$, the moment resistance of the joint, min{$M_{ip,1,Rd}$, $M_{w,Rd}$};
- $M^*_{j,Rd}$, the moment resistance of the joint without k_{HSS}; min{$M^*_{ip,1,Rd}$, $M_{w,Rd}$};
- $\varphi_{lim,3\%}$, the rotation limit.

Table 5. Theoretically calculated values.

Specimen	β	a_w / $a_{w,fs}$	$M^*_{ip,1,Rd}$ [kNm]	k_{HSS}	$M_{ip,1,Rd}$ [kNm]	$M_{w,Rd}$ [kNm]	$M^*_{j,Rd}$ [kNm]	$M_{j,Rd}$ [kNm]	Limiting factor	$\varphi_{lim,3\%}$ [rad]
S420_S420_a6	0.66	0.51	20.0	0.9	18.0	17.6	17.6	17.6	Weld	0.090
S500_S420_a6	0.67	0.51	24.1	0.8	19.3	17.6	17.6	17.6	Weld	0.089
S500_S500_a6	0.67	0.47	24.1	0.8	19.3	19.8	19.8	19.3	Chord	0.089
S700_S420_a6	0.67	0.51	30.1	0.8	24.1	17.6	17.6	17.6	Weld	0.090
S700_S500_a6	0.67	0.47	30.1	0.8	24.1	19.7	19.7	19.7	Weld	0.090
S700_S500_a6_WiPF	0.67	0.47	30.1	0.8	24.1	19.8	19.8	19.8	Weld	0.090
S700_S700_a6	0.80	0.45	52.6	0.8	42.1	39.1	39.1	39.1	Weld	0.075
S420_S420_a10	0.67	0.84	20.1	0.9	18.1	29.4	20.1	18.1	Chord	0.091
S500_S420_a10	0.67	0.84	24.1	0.8	19.3	29.3	24.1	19.3	Chord	0.090
S500_S500_a10	0.67	0.78	24.1	0.8	19.3	32.9	24.1	19.3	Chord	0.089
S700_S420_a10	0.67	0.84	29.9	0.8	23.9	29.3	29.3	23.9	Chord	0.091
S700_S500_a10	0.67	0.78	30.1	0.8	24.0	33.0	30.1	24.0	Chord	0.090
S700_S500_a10_WiPF	0.67	0.78	30.0	0.8	24.0	33.0	30.0	24.0	Chord	0.090
S700_S700_a10	0.80	0.76	53.1	0.8	42.5	65.4	53.1	42.5	Chord	0.075
S420_S420_1/2v	0.67	-	20.2	0.9	18.2	33.0	20.2	18.2	Chord	0.090
S500_S420_1/2v	0.67	-	24.2	0.8	19.3	33.0	24.2	19.3	Chord	0.090
S500_S500_1/2v	0.67	-	24.2	0.8	19.3	37.3	24.2	19.3	Chord	0.089
S700_S420_1/2v	0.67	-	30.0	0.8	24.0	32.8	30.0	24.0	Chord	0.091
S700_S500_1/2v	0.67	-	30.4	0.8	24.3	37.5	30.4	24.3	Chord	0.089
S700_S700_1/2v	0.81	-	54.6	0.8	43.7	74.1	54.6	43.7	Chord	0.075

Experimental plastic resistance $M_{pl,exp}$ was compared to theoretical moment resistance based on the chord face failure $M_{ip,1,Rd}$, with and without k_{HSS}. Similarly, the rotation corresponding to the ultimate moment resistance was compared to the rotation limit $\varphi_{lim,3\%}$. Table 6 provides the summary of the comparative analysis.

Table 6. Comparison of the experimental and theoretical values: value, average (and the standard deviation).

Specimen	β	a_w / $a_{w,fs}$	$M^*_{ip,1,Rd}$ / $M_{pl,exp}$		$M_{ip,1,Rd}$ / $M_{pl,exp}$		$\varphi_{lim,3\%}$ / φ_u	
S420_S420_a6	0.66	0.51	0.95		0.85		0.33	
S500_S420_a6	0.67	0.51	0.99		0.79		0.38	
S500_S500_a6	0.67	0.47	0.96	0.98	0.77	0.79	0.39	0.45
S700_S420_a6	0.67	0.51	1.09	(0.07)	0.87	(0.06)	0.43	(0.14)
S700_S500_a6	0.67	0.47	1.02		0.82		0.32	
S700_S500_a6_WiPF	0.67	0.47	0.96		0.77		0.61	
S700_S700_a6	0.80	0.45	0.86		0.69		0.68	
S420_S420_a10	0.67	0.84	0.64		0.57		0.34	
S500_S420_a10	0.67	0.84	0.69		0.55		0.30	
S500_S500_a10	0.67	0.78	0.65	0.71	0.52	0.58	0.44	0.46
S700_S420_a10	0.67	0.84	0.78	(0.07)	0.62	(0.05)	0.45	(0.14)
S700_S500_a10	0.67	0.78	0.66		0.53		0.52	
S700_S500_a10_WiPF	0.67	0.78	0.80		0.64		0.45	
S700_S700_a10	0.80	0.76	0.76		0.61		0.74	
S420_S420_1/2v	0.67	-	1.09		0.98		0.41	
S500_S420_1/2v	0.67	-	1.15		0.92		0.39	
S500_S500_1/2v	0.67	-	1.15	1.16	0.92	0.94	0.51	0.53
S700_S420_1/2v	0.67	-	1.24	(0.05)	0.99	(0.03)	0.57	(0.19)
S700_S500_1/2v	0.67	-	1.15		0.92		0.42	
S700_S700_1/2v	0.81	-	1.17		0.93		0.88	

Discussion

Resistance

In respect of joint resistance, attention is paid to the following two issues: the need for the reduction factors k_{HSS} in case of plastic resistance (chord face failure) and other possible improvements to the resistance calculation. The results show that theoretical resistance considerably underestimates experimental plastic resistance for the joints with a10 fillet welds ($a_w/a_{w,fs}$ = 0.76…0.84) with the average $M_{ip,1,Rd}$ / $M_{pl,exp}$ ratio of 0.58. Even without the reduction, the average ratio is 0.71. This observation justifies the need for the reduction coefficient k_{HSS} for joints with large fillet welds ($a_w/a_{w,fs} \geq 0.75$).

For joints with a6 fillet welds ($a_w/a_{w,fs}$ = 0.45-0.51), the situation is not so straightforward. With the reduction coefficient k_{HSS}, all the joints are on the safe side, with the average $M_{ip,1,Rd} / M_{pl,exp}$ ratio of 0.79. When the reduction is not taken into account, the average $M^*_{ip,1,Rd} / M_{pl,exp}$ ratio is 0.98, which also yields safe results. However, the ratio exceeds 1.0 for two cases, S700_S420_a6 and S700_S500_a6 (both have the chord made of S700). This implies the following rule: for joints with $0.45 \leq a_w/a_{w,fs} < 0.75$, no reduction may be needed, when the steel grade is below S700 (S500 can be the optimal limit). For steel grade S700, the reduction is needed; however, k_{HSS} = 0.9 seems to be sufficient, instead of the conservative value of 0.8. This conclusion is in line with the observations of [6].

Regarding the butt-welded joints, without reduction their theoretical moment resistance exceeds the experimental values in all cases, with an average $M^*_{ip,1,Rd} / M_{pl,exp}$ ratio of 1.16. At the same time, taking into account the reduction factors, all the joints show safe performance, with the average $M_{ip,1,Rd} / M_{pl,exp}$ ratio being 0.94. Therefore, for butt-welded joints, reduction is required, provided that butt welds are completed as in this research and their resistance is calculated as in this paper. Table 7 contains a summary of the observations regarding the reduction coefficients.

Table 7. Summary of the reduction coefficients observations.

Rule	Reduction factor for $f_y \geq 355$ MPa	Reduction factor for 460 MPa $\leq f_y \leq$ 700 MPa
Reference	EN 1993-1-8:2005, clause 7.1.1(4); CIDECT Design Guide No.3, clause 1.2.1	EN 1993-1-12:2007, clause 2.8; CIDECT Design Guide No.3, clause 1.2.1
Existing value	0.9	0.8
Possible value:		
Butt welds	0.9	0.8
Fillet welds, $a_w/a_{w,fs} \geq 0.75$	1.0	1.0
Fillet welds, $0.45 \leq a_w/a_{w,fs} < 0.75$	1.0	1.0 for S500 0.9 for S700 Linear interpolation between

Different findings for joints with various welds can be explained by the fact that experimental plastic resistance directly depends on the fillet weld size. Table 4 and Fig. 10 clearly show that the joints with fillet welds have higher experimental resistance than the joints with butt welds and the same geometry and material properties (compare, e.g., S420_S420_1/2v, S420_S420_a6 and S420_S420_a10). However, EN 1993-1-8:2005 does not take this phenomenon into account and provides the same theoretical resistance for joints with different weld types and sizes, as can be seen in Table 5 (slight differences of $M_{ip,1,Rd}$ are caused by deviations in the measured dimensions of the specimens). For this reason, the ratio $M_{ip,1,Rd} / M_{pl,exp}$ is found to be unsafe for the joints with butt welds, requiring reduction; close to 1.0 for the joints with a6 fillet welds, requiring partial reduction; and very conservative for the joints with a10 fillet welds, justifying no reduction for such joints. If full-strength welds were used, the underestimation would be even greater.

To develop more generalized conclusions, the theoretical resistance of RHS joints should first be calculated incorporating the improving effect of fillet welds. This effect can be taken into account, e.g., by increasing β by means of some simple equation, as has been proposed for initial stiffness in [50]. However, such an approach has to be applied carefully: if the enlarged β is used in the cases with $\beta = 0.8$ (S700_S700_a6 and S700_S700_a10), it might exceed the limit of $\beta \leq 0.85$, thus making the chord face failure calculation invalid and requiring the resistance to be calculated based on chord side-wall crushing and brace failure. It should be noted that this paper considers the reduction factors for the joints with $\beta \leq 0.85$, i.e., when the failure of the joint is caused by the bending of the chord top face. When other failure modes prevail, the conclusions can be different.

Application of MAG Wise welding did not yield noticeable improvements in the performance of the joints. Moreover, in the case of a6 joints (compare S700_S500_a6 and S700_S500_a6_WiPF), it decreased their ultimate bending resistance by 21%, in the case of a10 joints (compare S700_S500_a10 and S700_S500_a10_WiPF) by 11%.

Stiffness

The initial rotational stiffness of joints with an a10 fillet weld was found to be clearly higher than that of joints with a6 fillet welds (by 42% on average) and also 1/2v butt welds (by 63% on average). The results clearly show that fillet welds significantly affect not only the moment resistance of joints, but also their initial rotational stiffness. To take this effect into account in the design, a possible solution has been proposed in [50]. A similar improving effect was also observed for hardening stiffness in these tests.

Application of MAG Wise welding did not bring noticeable improvements in the rotational stiffness of the joints. Moreover, in the case of a10 fillet welds (compare S700_S500_a10 and S700_S500_a10_WiPF) it decreased both the initial stiffness and the hardening stiffness by 15% and 6% respectively.

Ductility

The results show that the experimental ultimate rotation capacity of all the tested joints clearly exceeded the $3\%b_0$ deformation limit, provided that no full-strength fillet welds were used. According to Table 6, the ratio $\varphi_{lim,3\%} / \varphi_u$ lies in the range of 0.33…0.61 for the joints with $\beta = 0.67$ and 0.68…0.88 for the joints with $\beta = 0.80$. Such a considerable margin justifies the use of welds smaller than full-strength fillet welds if they provide sufficient resistance.

Conclusions

The moment-rotation behavior of all the tested specimens was found to follow the typical moment-rotation response for joints with $\beta \leq 0.85$. The rotation capacity of all the specimens complies with the requirements for tubular joints, even using welds smaller than full-strength welds. This indicates that full-strength fillet welds are not needed in these joints and in this loading condition.

The experimental results show that the size of fillet welds has a significant influence on the structural behavior of joints, increasing their bending resistance and rotational stiffness. To avoid overly conservative results, such phenomenon should be taken into account in the design of tubular joints.

There is no single conclusion concerning the relevance of the reduction factors for the bending resistance of HSS joints limited by chord face failure. This issue is complicated by the fact that the current design rules do not consider the improving effect of fillet welds on the structural behavior of tubular joints. If this influence is neglected, the reduction is necessary only for butt-welded joints, as well as for joints with small fillet welds ($0.45 \leq a_w/a_{w,fs} < 0.75$) and made of steel grades higher than S500. It should be noted that these conclusions are based on the tests carried out, i.e., for square hollow sections of 8 mm

thickness ($2\gamma = b_0/t_0 = 18.75$). More tests are required to establish the reliability of these observations in relation to joints with other 2γ ratio, as well as for rectangular hollow section joints. Moreover, further investigations are needed to specify the relevance of the reduction factors k_{HSS} for the bending resistance based on other failure modes, as well as for the design of welds.

Acknowledgements

The authors appreciate the financial support of the city of Hämeenlinna. The authors would like to thank SSAB Europe Oy for providing the high strength steel tubular materials and Tavastia Vocational College for manufacturing the specimens. The financial support of the Tekes project FIMECC/Digimap is also gratefully acknowledged.

References

[1] J. Raoul, H.-P. Günther, *Use and application of high-performance steels for steel structures (SED 8)*, 8. Iabse, Zürich, Switzerland, 2005.

[2] (CEN) European Committee for Standardization, *Eurocode 3. Design of steel structures, Part 1-12: Additional rules for the extension of EN 1993 up to steel grades S 700 (EN 1993-1-12: 2007)*. Brussels, 2007.

[3] (CEN) European Committee for Standardization, *Eurocode 3. Design of steel structures, Part 1–8: Design of joints (EN 1993-1-8:2005)*. Brussels, 2005.

[4] J.A. Packer, J. Wardenier, X.-L. Zhao, G.J. van der Vegte, Y. Kurobane, Design guide for rectangular hollow section (RHS) joints under predominantly static loading, CIDECT Des. Guid. No. 3, 2nd Ed. CIDECT, Geneva, Switz. (2009) .

[5] X.-L. Zhao, A. Heidarpour, L. Gardner, Recent developments in high-strength and stainless steel tubular members and connections, Steel Constr. 7(2) (2014) 65–72.

[6] M. Feldmann, N. Schillo, S. Schaffrath, K. Virdi, T. Björk, N. Tuominen, M. Veljkovic, M. Pavlovic, P. Manoleas, M. Heinisuo, K. Mela, P. Ongelin, I. Valkonen, J. Minkkinen, J. Erkkilä, E. Pétursson, M. Clarin, A. Seyr, L. Horváth, B. Kövesdi, P. Turán, B. Somodi, *Rules on high strength steel*. Luxembourg: Publications Office of the European Union, 2016.

[7] H. Jiao, X.-L. Zhao, A. Lau, Hardness and compressive capacity of longitudinally welded very high strength steel tubes, J. Constr. Steel Res. 114 (2015) 405–416.

[8] F. Javidan, A. Heidarpour, X.-L. Zhao, C.R. Hutchinson, J. Minkkinen, Effect of weld on the mechanical properties of high strength and ultra-high strength steel tubes in fabricated hybrid sections, Eng. Struct. 118 (2016) 16–27.

[9] M. Pirinen, *The Effects of Welding Heat Input on the Usability of High Strength Steels in Welded Structures*. *Doctor of Science Thesis*. Lappeenranta: Lappeenranta University of Technology, 2013.

[10] M. Dunđer, I. Samardžić, Š. Klarić, Influence of Cooling Time Δt8/5 on Welded Joint Properties of the Thermal Cycle Simulated TStE 420 Specimens, Tech. Gaz. 14(1–2) (2007) 47–57.

[11] S. Rakentamismääräyskokoelma, *Rakenteiden lujuus ja vakaus. Teräsrakenteet*. 2017.

[12] P. Ongelin, I. Valkonen, *SSAB Domex Tube. Structural hollow sections. EN 1993 - Handbook 2016*. SSAB Europe Oy, 2016.

[13] D. Grotmann, G. Sedlacek, *Rotational stiffness of welded RHS beam-to-column joints. Cidect 5BB-8/98*. Aachen: RWTH-Aachen, 1998.

[14] R.L. Brockenbrough, Strength of Square-Tube Connections under Combined Loads, J. Struct. Div. 98(12) (1972) 2753–2768.

[15] R.M. Korol, M. El-Zanaty, F.J. Brady, Unequal width connections of square hollow sections in Vierendeel trusses, Can. J. Civ. Eng. 4(2) (1977) 190–201.

[16] H. Kanatani, K. Fujiwara, M. Tabuchi, T. Kamba, *Bending tests on T-joints of RHS chord and*

RHS or H-shape branch. CIDECT Programme 5AF. 1981.
[17] J.A. Yura, I.F. Edwards, N. Zettlemoyer, Ultimate Capacity of Circular Tubular Joints, J. Struct. Div. 107(10) (1981) 1965–1984.
[18] J. Wardenier, *Hollow Section Joints*. Delft: Delft University of Technology, 1982.
[19] (IIW) International Institute of Welding, *ISO 14346:2013. Static design procedure for welded hollow-section joints - Recommendations*. 2013.
[20] K. Ishida, T. Ono, M. Iwata, Ultimate strength formula for joints of new truss system using rectangular hollow sections, Proceedings of 5th International Symposium on Tubular Structures, 1993, pp. 511–518.
[21] T. Ono, M. Iwata, K. Ishida, An experimental study on joints of new truss system using rectangular hollow sections, Proceedings of 4th International Symposium on Tubular Structures, 1991, pp. 344–353.
[22] M. Tabuchi, H. Kanatani, T. Kamba, The local strength of welded RHS T joints subjected to bending moment, CIDECT Rep. 5AF-84/5E. (1984) .
[23] J. Szlendak, Beam-column welded RHS connections, Thin-Walled Struct. 12(1) (1991) 63–80.
[24] J.A. Packer, Moment connections between rectangular hollow sections, J. Constr. Steel Res. 25(1–2) (1993) 63–81.
[25] Y. Yu, *The static strength of uniplanar and multiplanar connections in rectangular hollow sections. Doctoral Dissertation*. Delft: Delft University of Technology, 1997.
[26] L.H. Lu, G.D. De Winkel, Y. Yu, J. Wardenier, Deformation limit for the ultimate strength of hollow section joints, 6th International Symposium on Tubular Structures, Melbourne, Australia, 1994, pp. 341–347.
[27] X.-L. Zhao, Deformation limit and ultimate strength of welded T-joints in cold-formed RHS sections, J. Constr. Steel Res. 53(2) (2000) 149–165.
[28] A.D. Christitsas, D.T. Pachoumis, C.N. Kalfas, E.G. Galoussis, FEM analysis of conventional and square bird-beak SHS joint subject to in-plane bending moment — experimental study, J. Constr. Steel Res. 63(10) (2007) 1361–1372.
[29] M. Fadden, D. Wei, J. McCormick, Cyclic Testing of Welded HSS-to-HSS Moment Connections for Seismic Applications, J. Struct. Eng. 141(2) (2015) 4014109.
[30] F. Mang, O. Bucak, H. Stauf, Fatigue behaviour of welded hollow section joints and their connections made of high-strength steels, Proceedings of the Third (1993) International Offshore and Polar Engineering Conference, 1993, pp. 104–116.
[31] D. Anderson, E.L. Hines, S.J. Arthur, E.L. Eiap, Application of artificial neural networks to the prediction of minor axis steel connections, Comput. Struct. 63(4) (1997) 685–692.
[32] D.E. Grierson, L. Xu, Design optimization of steel frameworks accounting for semi-rigid connections, , in *Optimization of Large Structural Systems, Volume II*, G. I. N. Rozvany, Ed. Dordrecht: Kluwer Academic Publisher, 1993, 873–881.
[33] L.M.C. Simoes, Optimization of frames with semi-rigid connections, Comput. Struct. 60(4) (1996) 531–539.
[34] K. Weynand, J.-P. Jaspart, M. Steenhuis, Economy studies of steel building frames with semi-rigid joints, J. Constr. Steel Res. 46(1–3) (1998) 85.
[35] J. Haapio, T. Jokinen, M. Heinisuo, Cost simulations of steel frames with semi-rigid joints using product model techniques, Proceedings of Eurosteel 2011, 2011, pp. 2151–2156.
[36] K. Bzdawka, Optimization of Office Building Frame with Semi-Rigid Joints in Normal and Fire Conditions, PhD Thesis, Tampere Univ. Technol. Publ. 1038. (2012) .
[37] H. Boel, *Buckling Length Factors of Hollow Section Members in Lattice Girders. Ms Sci thesis*. Eindhoven: Eindhoven University of Technology, 2010.
[38] H.H. Snijder, H.D. Boel, J.C.D. Hoenderkamp, R.C. Spoorenberg, Buckling length factors for welded lattice girders with hollow section braces and chords, Proc. Eurosteel 2011. (2011) 1881–

1886.
[39] M. Heinisuo, Ä. Haakana, Buckling of members of welded tubular truss, Nord. Steel Constr. Conf. 2015. (2015) .
[40] M. Garifullin, S. Pajunen, K. Mela, M. Heinisuo, J. Havula, Initial in-plane rotational stiffness of welded RHS T joints with axial force in main member, J. Constr. Steel Res. 139 (2017) 353–362.
[41] (CEN) European Committee for Standardization, *Eurocode 3. Design of steel structures. Part 1-5: Plated structural elements (EN 1993-1-5:2006)*. Brussels, 2006.
[42] R. Spangemacher, G. Sedlacek, On the development of a computer simulator for tests of steel structures, Constr. Steel Des. World Dev. (1992) 593–611.
[43] W. Dahl, P. Langenberg, G. Sedlacek, R. Spangemacher, *Elastisch-plastisches Verhalten von Stahlkonstruktionen- Anforderungen und Werkstoffkennwerte*. Luxembourg: EUR, 1993.
[44] (CEN) European Committee for Standardization, *Eurocode 3: Design of steel structures, Part 1-1: General rules and rules for buildings (EN 1993-1-1:2005)*. Brussels, 2005, 2005.
[45] D. Beg, E. Zupančič, I. Vayas, On the rotation capacity of moment connections, J. Constr. Steel Res. 60(3–5) (2004) 601–620.
[46] (CEN) European Committee for Standardization, *Eurocode 8. Design of structures for earthquake resistance, Part 1: General rules, seismic actions and rules for buildings (EN 1998-1:2004)*. Brussels, 2004, 2004.
[47] S. Wilkinson, G. Hurdman, A. Crowther, A moment resisting connection for earthquake resistant structures, J. Constr. Steel Res. 62(3) (2006) 295–302.
[48] N. Kosteski, J.A. Packer, R.S. Puthli, A finite element method based yield load determination procedure for hollow structural section connections, J. Constr. Steel Res. 59(4) (2003) 453–471.
[49] (CEN) European Committee for Standardization, *Welding and allied processes – Types of joint preparation – Part 1: Manual metal arc welding, gas-shielded metal arc welding, gas welding, TIG welding and beam welding of steels (ISO 9692-1:2013)*. Brussels, 2013, 2013.
[50] M. Heinisuo, M. Garifullin, T. Jokinen, T. Tiainen, K. Mela, Surrogate modeling for rotational stiffness of welded tubular Y-joints, Proceedings of The Eighth International Workshop on Connections in Steel Structures (Connections VIII), 2016, pp. 285–294.

Appendix. Moment-rotation curves

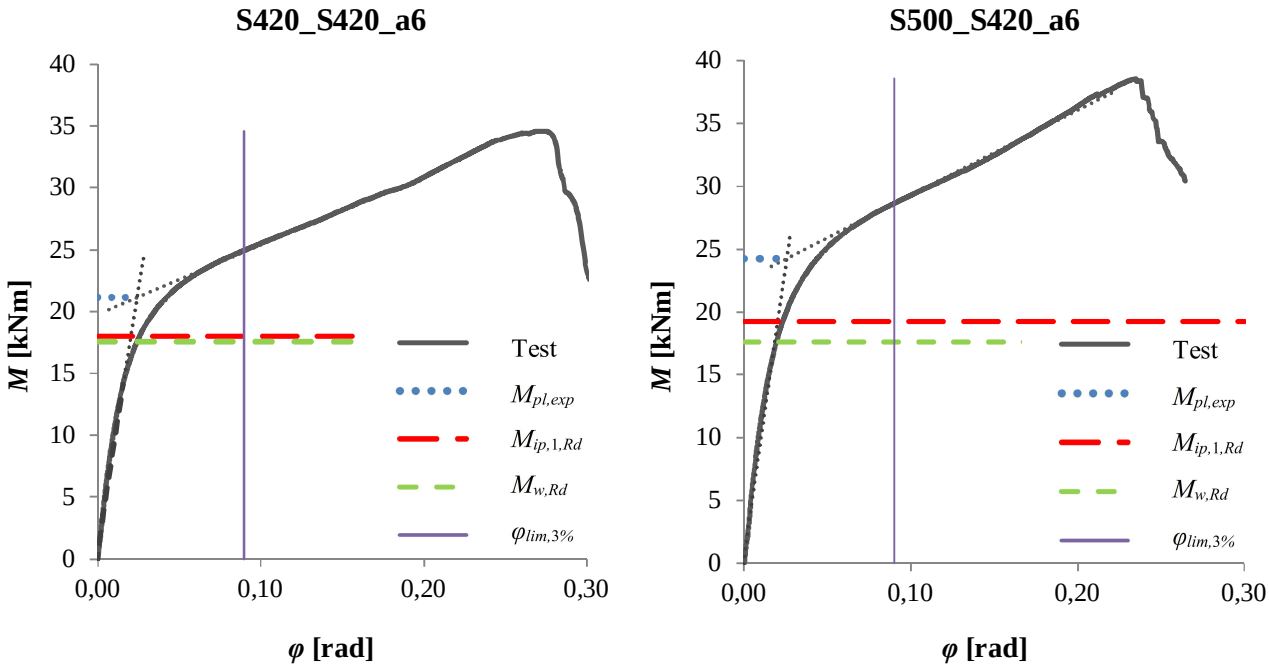

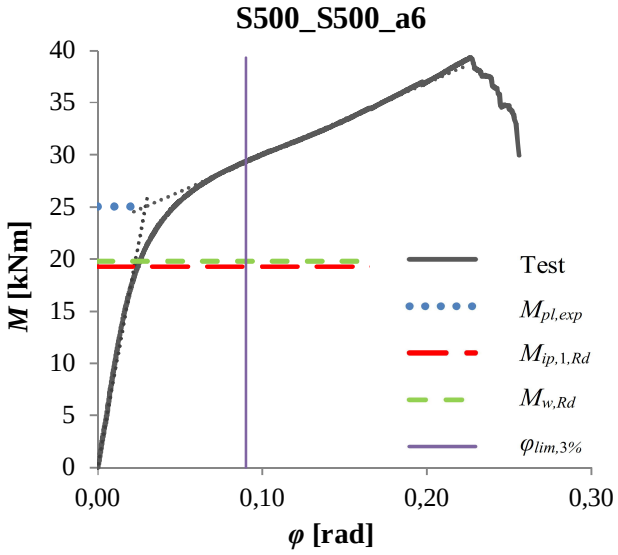
S500_S500_a6
M [kNm]
φ [rad]
Test
$M_{pl,exp}$
$M_{ip,1,Rd}$
$M_{w,Rd}$
$\varphi_{lim,3\%}$

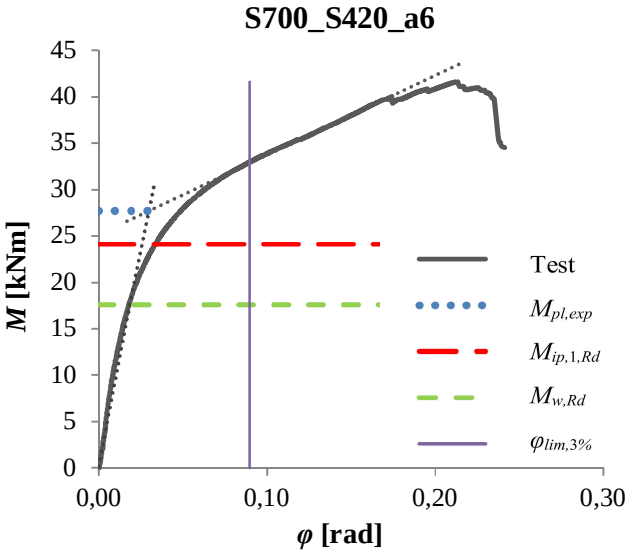
S700_S420_a6
M [kNm]
φ [rad]
Test
$M_{pl,exp}$
$M_{ip,1,Rd}$
$M_{w,Rd}$
$\varphi_{lim,3\%}$

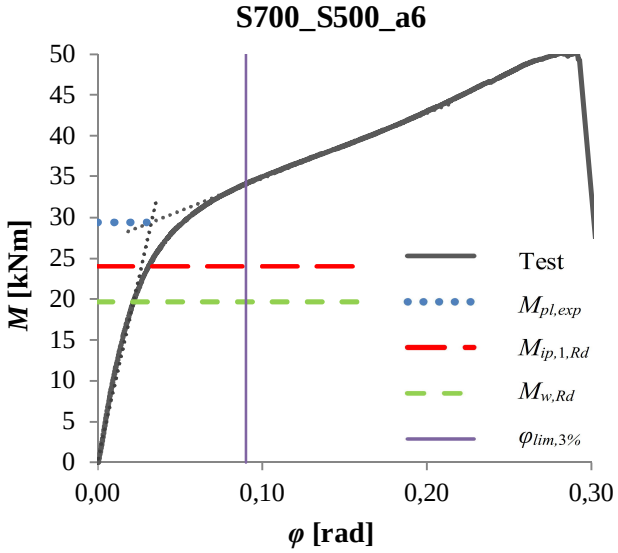
S700_S500_a6
M [kNm]
φ [rad]
Test
$M_{pl,exp}$
$M_{ip,1,Rd}$
$M_{w,Rd}$
$\varphi_{lim,3\%}$

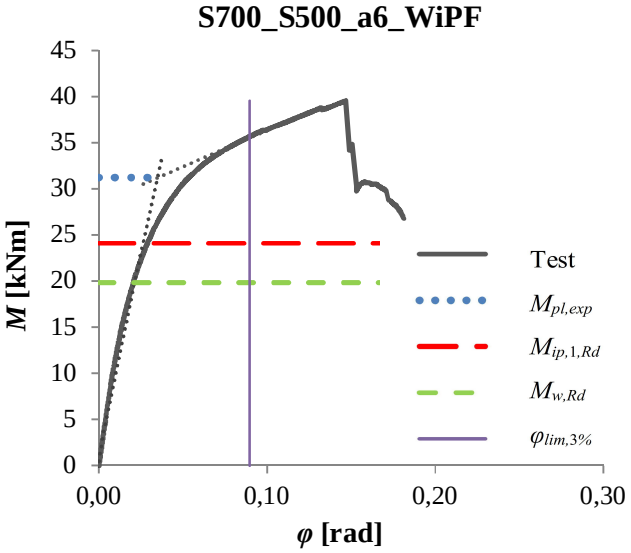
S700_S500_a6_WiPF
M [kNm]
φ [rad]
Test
$M_{pl,exp}$
$M_{ip,1,Rd}$
$M_{w,Rd}$
$\varphi_{lim,3\%}$

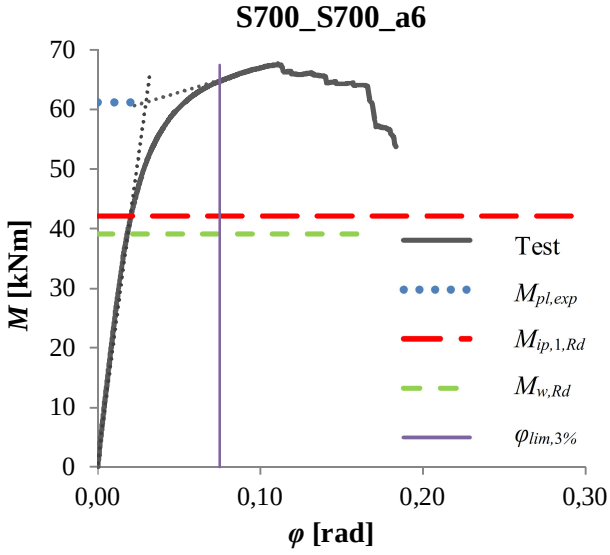
S700_S700_a6
M [kNm]
φ [rad]
Test
$M_{pl,exp}$
$M_{ip,1,Rd}$
$M_{w,Rd}$
$\varphi_{lim,3\%}$

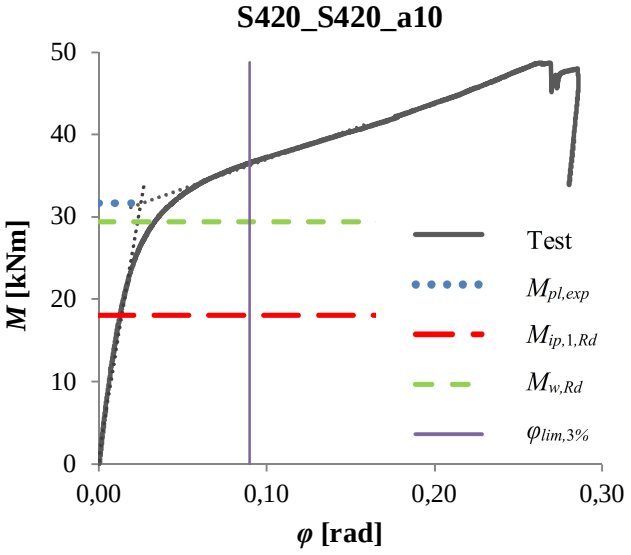
S420_S420_a10
M [kNm]
φ [rad]
Test
$M_{pl,exp}$
$M_{ip,1,Rd}$
$M_{w,Rd}$
$\varphi_{lim,3\%}$

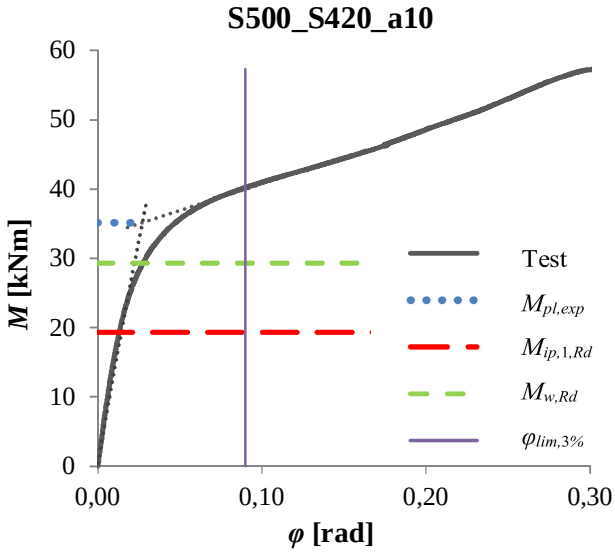
S500_S420_a10
M [kNm]
φ [rad]
Test
$M_{pl,exp}$
$M_{ip,1,Rd}$
$M_{w,Rd}$
$\varphi_{lim,3\%}$

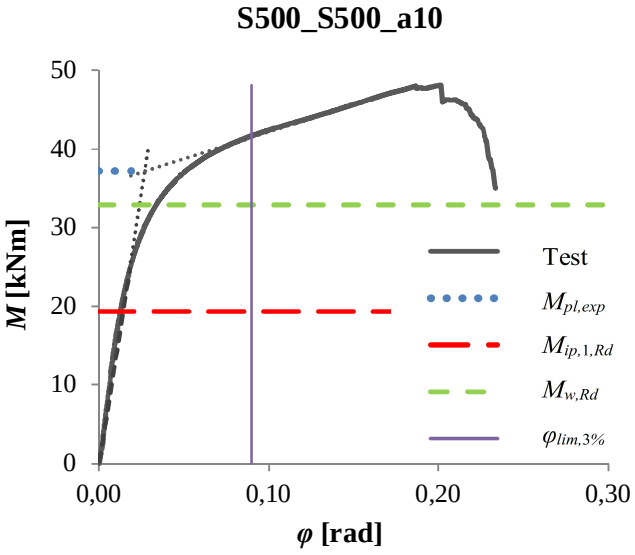
S500_S500_a10
M [kNm]
φ [rad]
Test
$M_{pl,exp}$
$M_{ip,1,Rd}$
$M_{w,Rd}$
$\varphi_{lim,3\%}$

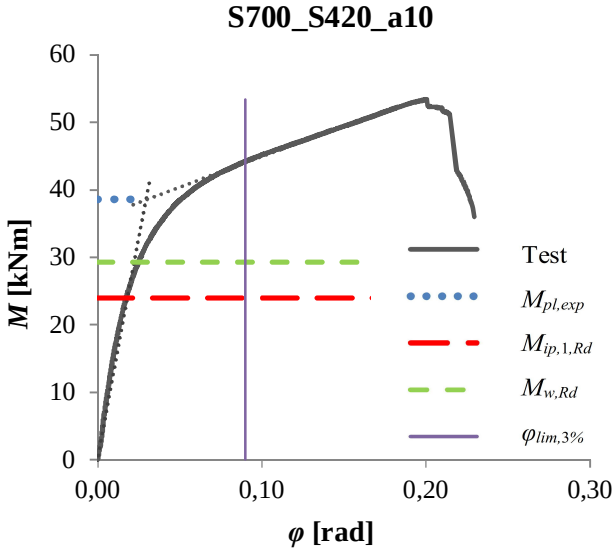
S700_S420_a10
M [kNm]
φ [rad]
Test
$M_{pl,exp}$
$M_{ip,1,Rd}$
$M_{w,Rd}$
$\varphi_{lim,3\%}$

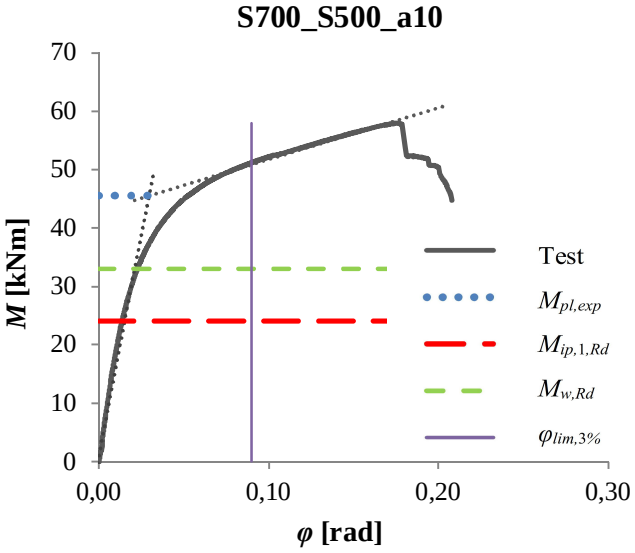
S700_S500_a10
M [kNm]
φ [rad]
Test
$M_{pl,exp}$
$M_{ip,1,Rd}$
$M_{w,Rd}$
$\varphi_{lim,3\%}$

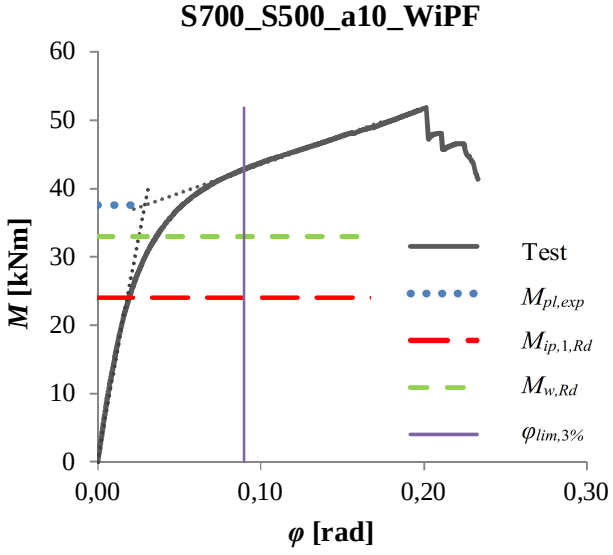
S700_S500_a10_WiPF
M [kNm]
φ [rad]
Test
$M_{pl,exp}$
$M_{ip,1,Rd}$
$M_{w,Rd}$
$\varphi_{lim,3\%}$

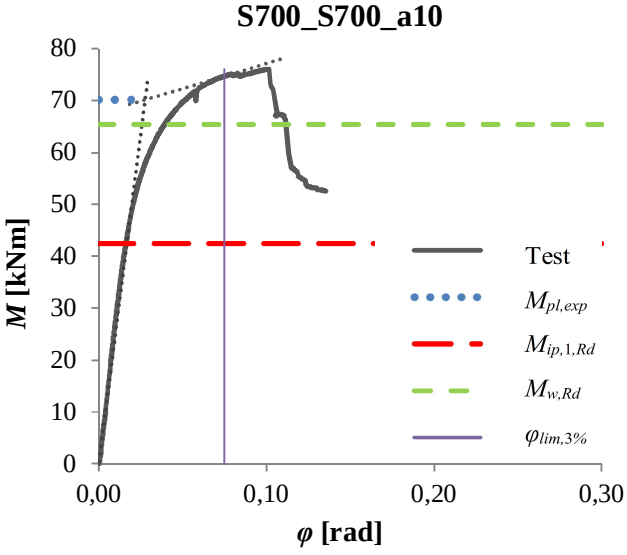
S700_S700_a10
M [kNm]
φ [rad]
Test
$M_{pl,exp}$
$M_{ip,1,Rd}$
$M_{w,Rd}$
$\varphi_{lim,3\%}$

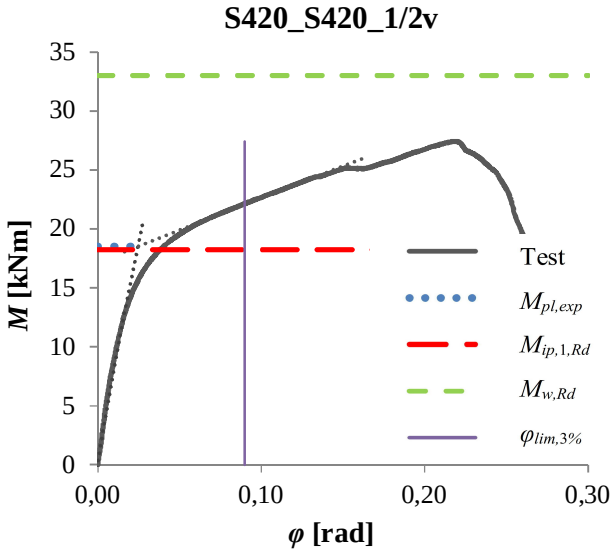
S420_S420_1/2v
M [kNm]
φ [rad]
Test
$M_{pl,exp}$
$M_{ip,1,Rd}$
$M_{w,Rd}$
$\varphi_{lim,3\%}$

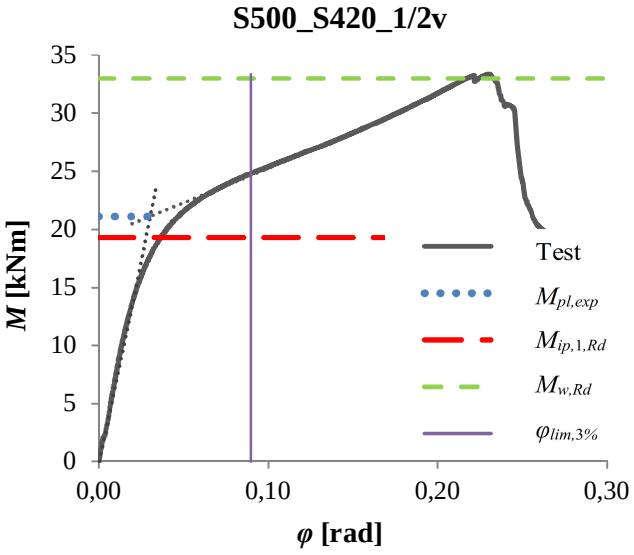
S500_S420_1/2v
M [kNm]
φ [rad]
Test
$M_{pl,exp}$
$M_{ip,1,Rd}$
$M_{w,Rd}$
$\varphi_{lim,3\%}$

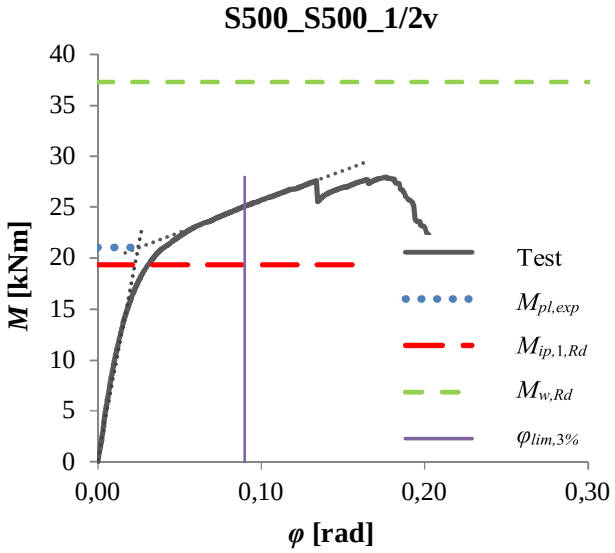
S500_S500_1/2v
M [kNm]
φ [rad]
Test
$M_{pl,exp}$
$M_{ip,1,Rd}$
$M_{w,Rd}$
$\varphi_{lim,3\%}$

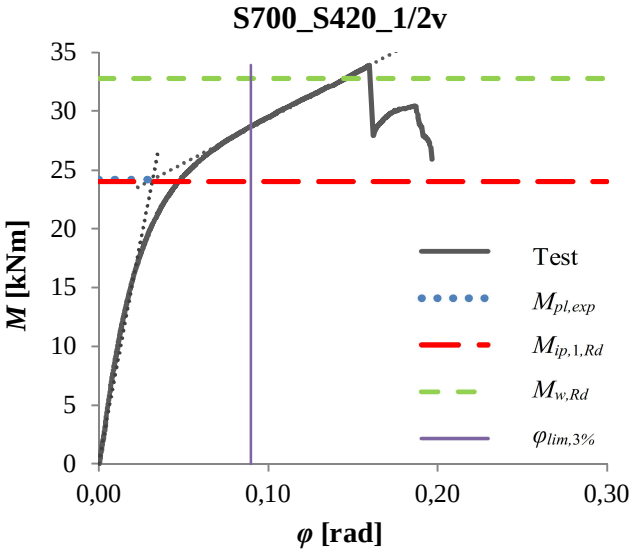
S700_S420_1/2v
M [kNm]
φ [rad]
Test
$M_{pl,exp}$
$M_{ip,1,Rd}$
$M_{w,Rd}$
$\varphi_{lim,3\%}$

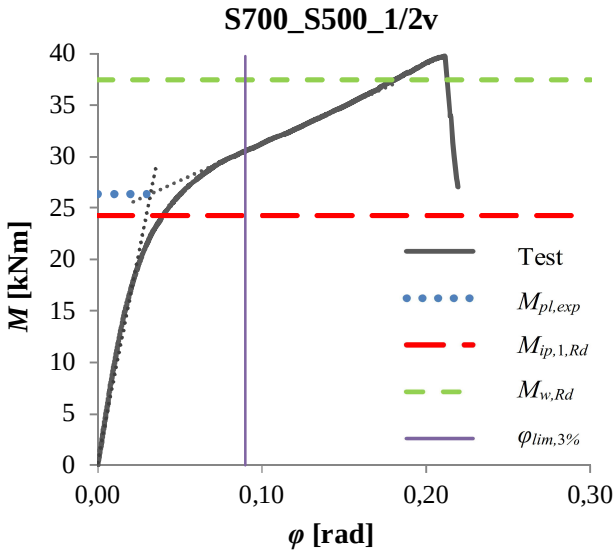
S700_S500_1/2v
M [kNm]
φ [rad]
Test
$M_{pl,exp}$
$M_{ip,1,Rd}$
$M_{w,Rd}$
$\varphi_{lim,3\%}$

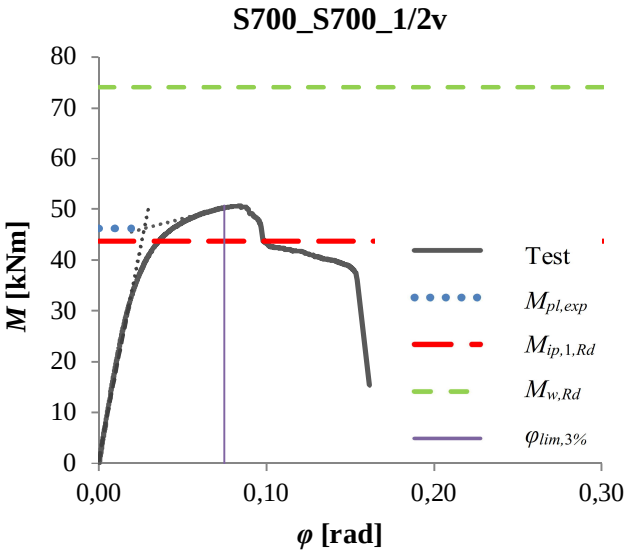
S700_S700_1/2v
M [kNm]
φ [rad]
Test
$M_{pl,exp}$
$M_{ip,1,Rd}$
$M_{w,Rd}$
$\varphi_{lim,3\%}$